

A modification of the classical Ekman model accounting for the Stokes drift and stratification effects

Jaak Heinloo · Aleksander Toompuu

Received: 22 December 2010 / Accepted: 18 April 2011 / Published online: 1 May 2011
© Springer Science+Business Media B.V. 2011

Abstract A modification of the classical Ekman model of oceanic wind-driven currents including the Stokes drift and stratification effects is discussed. The modification is formulated as an application of turbulence mechanics accounting for the curvature effect of velocity fluctuation streamlines. It is shown that similar to the Stokes drift effect, the presence of a density jump layer (pycnocline) decreases the veering of the flow velocity vector at the surface from the direction of the wind stress. It is shown also that in the pycnocline the decrease of the norm of the velocity vector as well as its rotation with depth is smaller than in the regions adjacent to the pycnocline. If the Stokes drift and stratification effects are neglected, the model reduces to the classical Ekman solution with the coefficient of the turbulent shear viscosity replaced by an effective viscosity coefficient. The vertical distributions of velocity predicted by the modified model are compared with the velocity data measured in the Drake Passage and within the Long-Term Upper Ocean Study (LOTUS) in the North Atlantic.

Keywords Turbulence · Modeling · Ekman layer · Stratification · Stokes drift

1 Introduction

Based on the observed vertical structure of the velocity of wind-driven currents in the upper ocean, it has been argued that the observations deviate in several aspects from the structure predicted by the classical Ekman model [7]—a large component of the shear in the downwind direction near the surface turns less than predicted by the Ekman solution [33], the angle between the surface wind stress and the surface drift velocity vectors differs (in general) from $\pi/4$ [5], the velocity shear and stresses seem non-collinear [24], and the velocity rotational

J. Heinloo · A. Toompuu (✉)
Marine Systems Institute, Tallinn University of Technology,
Akadeemia tee 15A, 12618 Tallinn, Estonia
e-mail: alex@phys.sea.ee

J. Heinloo
e-mail: heinloo@phys.sea.ee

depth scale estimated from the observed data is claimed to exceed its e -folding depth scale by 2–3 times [2, 3, 24, 29–31, 33, 37, 38]. Several attempts such as utilizing a depth-varying and complex eddy viscosity [23–25] and accounting for the buoyancy and the Stokes drift effects [4, 27, 28, 39] have been undertaken to adjust the Ekman model to the observed differences. The present paper follows the same aim, though applying another theoretical background. Instead of utilizing the theoretical conceptions traditional in the field, this paper proceeds from turbulence mechanics modified to account for the effects of the curvature of the velocity fluctuation streamlines [10–12], hereafter referred to as the Theory of Rotationally Anisotropic Turbulence or the RAT theory (Sect. 2). The applications of the RAT theory [10–22, 35, 36] have so far proven this theory to be a tool complementing the variety of tools for discussing oceanographic and other related problems. Concerning the Ekman layer it is shown that the application of the RAT theory embraces the Stokes drift and stratification effects in one single model. The suggested single model explains the observed deviations from the predictions of the classical Ekman model indicated above.

For a negligible stratification effect, the outcome of the suggested model is compared with data observed in the Drake Passage adopted from [24] and if the stratification effect is assumed present (as judged from the type of the measured velocity profiles)—with the data observed within the Long-Term Upper Ocean Study (LOTUS) in the North Atlantic [33]. It is shown that even if the rotational depth scale of velocity can exceed its e -folding depth scale within the suggested model, for the data in [24] these scales appear rather close to each other.

2 Theoretical background

Let us consider the quantity

$$\mathbf{\Omega} = \langle \mathbf{v}' \times \mathbf{k} \rangle \quad (1)$$

with the dimension of angular velocity of rotation (Fig. 1). In Eq. 1 $\mathbf{v}' = \mathbf{v} - \mathbf{u}$, where \mathbf{v} is the vector of actual velocity and $\mathbf{u} = \langle \mathbf{v} \rangle$, the angular brackets denote statistical averaging and

$$\mathbf{k} = \frac{\partial \mathbf{e}}{\partial s},$$

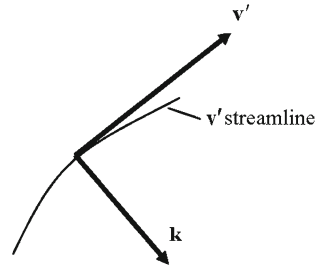
where $\mathbf{e} = \mathbf{v}'/v'$ ($v' = |\mathbf{v}'|$) and s is the length of the \mathbf{v}' streamline, denotes the vector of curvature of the velocity fluctuation streamline passing a flow point. The quantity $\mathbf{\Omega}$ defined by Eq. 1 determines the average angular velocity of rotation of medium particles at each flow field point due to the fluctuating constituent of the flow velocity with respect to the random curvature centre of the velocity fluctuation streamlines passing this point. Let us note that the quantity $\mathbf{\Omega}$ characterizes the fluctuating constituent of the flow field and therefore represents a flow field characteristic independent from the average velocity.

It is natural to couple the definition in Eq. 1 with the definition of the dynamic characteristic of motion

$$\mathbf{M} = \langle \mathbf{v}' \times \mathbf{R} \rangle = \langle R^2 \mathbf{v}' \times \mathbf{k} \rangle, \quad (2)$$

where $\mathbf{R} = \mathbf{k}/k^2$ ($k = |\mathbf{k}| = R^{-1}$, $R = |\mathbf{R}|$) is the curvature radius of velocity fluctuation streamline. The quantity \mathbf{M} has the sense of the average moment of momentum (or angular momentum) of medium particles at a flow field point due to the fluctuating constituent of the

Fig. 1 Representation of the fluctuating constituent of the velocity at a flow field point: \mathbf{v}' —velocity fluctuation and \mathbf{k} —vector of curvature of the velocity fluctuation streamline



flow field with respect to the random curvature centre of the velocity fluctuation streamlines passing this point.

Let us notice that the total turbulence energy $K = \frac{1}{2} \langle v'^2 \rangle$ of the turbulent flow characterized by $\mathbf{\Omega}$ and \mathbf{M} can be represented as

$$K = K^\Omega + K^0, \tag{3}$$

where

$$K^\Omega = \frac{1}{2} \mathbf{M} \cdot \mathbf{\Omega},$$

and

$$K^0 = \langle (\mathbf{v}' \times \mathbf{k})' \cdot (\mathbf{v}' \times \mathbf{R})' \rangle$$

in which the prime denotes fluctuation of the quantity; $(\mathbf{v}' \times \mathbf{k})' = \mathbf{v}' \times \mathbf{k} - \mathbf{\Omega}$, and $(\mathbf{v}' \times \mathbf{R})' = \mathbf{v}' \times \mathbf{R} - \mathbf{M}$. It is evident that for non-vanishing \mathbf{M} the turbulence energy constituent K^Ω in Eq. 3 does not vanish and therefore the rotation in the medium characterized by $\mathbf{\Omega}$ contributes (in general) to the dynamical and energetical processes in the medium. This inference relates the turbulent media characterized by the non-vanishing $\mathbf{\Omega}$ and \mathbf{M} to the class of micropolar fluids [1,6,8,9].

According to the theory of micropolar fluids [8], grounded on the general principles of continuum mechanics [32], the description of the situation constituted by Eqs. 1–3 should be subject to the conservation laws of momentum, moment of momentum, or angular momentum and energy K^0 . The RAT theory [12], which is applied in the following for a modification of the classical Ekman layer model, just derives the required equations from the Navier–Stokes equation and solves the imminent closure problem in agreement with the general closure technique applied in the context of the theory of micropolar fluids [1,6,8,9]. For the applied closure and for $\mathbf{\Omega} \equiv \mathbf{M} \equiv 0$ the RAT theory reduces to the conventional setup of the average turbulence description. Due to the latter property the RAT theory does not reject, but instead complements the conventional methods of the average turbulence description.

3 Model setup

3.1 The flow situation

Consider the flow in the upper layer of ocean in the Northern Hemisphere formed under a constant wind stress τ . The model is set up for the right-hand Cartesian coordinate system (x, y, z) rotating with the angular velocity $\boldsymbol{\omega}^0 = (0, 0, -f/2)$, where f is the Coriolis

parameter, with the coordinate z directed downward, $z = 0$ at the ocean surface, and the coordinate x directed in the downwind direction specifying the wind stress as $\boldsymbol{\tau} = (-\tau, 0, 0)$ with $\tau > 0$.

Similar to the setup of the classical Ekman model we shall assume for \mathbf{u} that

$$\mathbf{u} = [u_x(z), u_y(0), 0], \tag{4}$$

while

$$\mathbf{u} \rightarrow 0 \tag{5}$$

for $z \rightarrow \infty$, complemented within the discussed model by the following assumptions

$$\boldsymbol{\Omega} = [\Omega_x(z), \Omega_y(0), 0], \tag{6}$$

and

$$\boldsymbol{\Omega} \rightarrow 0 \tag{7}$$

for $z \rightarrow \infty$.

3.2 Model equations

For the flow situation specified above, the equations of the RAT theory coincide with the equations applied in [12] for the description of turbulent flows in plain channels with two exceptions—there is an additional Coriolis term in the equation of balance of the momentum and the body moment term $\rho \mathbf{m}$ ($\rho = 10^3 \text{ kg m}^{-3}$ is the medium characteristic density; \mathbf{m} is the density of the body moment acting on the medium due to the medium stratification) in the equation of balance of the moment of momentum. With these two exceptions the governing equations in the Boussinesq approximation can be written as

$$-\nabla p + \mu \frac{\partial^2}{\partial z^2} \mathbf{u} + \frac{1}{2} \nabla \times \boldsymbol{\sigma} + 2\rho \mathbf{u} \times \boldsymbol{\omega}^0 = 0, \tag{8}$$

$$\vartheta J \frac{\partial^2}{\partial z^2} \boldsymbol{\Omega} - \boldsymbol{\sigma} + 4\kappa \boldsymbol{\Omega} + \rho \mathbf{m} = 0 \tag{9}$$

where

$$\boldsymbol{\sigma} = 4\gamma(\boldsymbol{\Omega} - \boldsymbol{\omega}), \tag{10}$$

and the stratification effect is accounted for through [20]

$$\rho \mathbf{m} = -k_1 g \frac{\partial \rho^*}{\partial z} \boldsymbol{\Omega}, \tag{11}$$

in which ρ^* denotes the actual density of the medium. In Eqs. 8–11: $\boldsymbol{\omega} = 1/2 \nabla \times \mathbf{u}$ is the vorticity, p is the pressure, and J is the “effective moment of inertia” determined by $J = |\mathbf{M}| / |\boldsymbol{\Omega}|$. The coefficients $\mu, \gamma, \kappa, \vartheta$ (with the dimension $\text{ML}^{-1}\text{T}^{-1}$) have the following physical sense: μ is the coefficient of turbulent shear viscosity (quantifying the supply of energy K^0 from the energy of average flow); γ is the coefficient of rotational viscosity (coupling the average flow velocity and the medium internal rotation characterized by $\boldsymbol{\Omega}$); κ is the coefficient quantifying the energy transfer from the orientated turbulence constituent to the non-orientated turbulence constituent due to the cascading process; ϑ is the coefficient of diffusion of the moment of momentum \mathbf{M} ; k_1 (with the dimension of L^2T) is the proportionality coefficient quantifying the moment acting on the $\boldsymbol{\Omega}$ -field due to the

stratification and $g = |\mathbf{g}|$, where \mathbf{g} is the acceleration due to gravity. All medium coefficients in Eqs. 8–11, as well as J are treated as constants. Let us note that for $\gamma = 0$ Eq. 8 reduces to the respective equation of the classical Ekman model while for $\rho\mathbf{m} = 0$ and for $\mathbf{\Omega}$ equalized with the vorticity Eq. 9 reduces to the equation reflecting the Stokes drift effect. The boundary conditions for Eqs. 8 and 9 at $z = 0$ are specified as

$$\mu \frac{\partial u_x}{\partial z} - \frac{1}{2}\sigma_y = -\tau, \mu \frac{\partial u_y}{\partial z} + \frac{1}{2}\sigma_x = 0, \mathbf{\Omega} = \mathbf{\Omega}(0), \tag{12}$$

in the following we assume that the turbulent motion receives energy through an energy cascade excluding the supply of energy K^0 immediately from the average flow. In terms of the coefficients μ and γ this assumption is formalized by neglecting the shear viscosity effects in respect to the rotational viscosity effect, i.e., by neglecting the terms in (8) and (12) proportional to the shear viscosity μ .

3.3 Analysis of the model

3.3.1 Introductory notes

(a) With the simplifying assumption adopted, Eqs. 8, 9 and 12 can be rewritten in the form

$$-\tilde{\nabla} p + \gamma \tilde{u}'' + 2i\gamma \tilde{\Omega}' + i\rho f \tilde{u} = 0, \tag{13}$$

$$\vartheta J \tilde{\Omega}'' - 4(\gamma + \kappa)(1 + S)\tilde{\Omega} + 2i\gamma \tilde{u}' = 0, \tag{14}$$

$$\gamma \tilde{u}'(0) + 2i\gamma \tilde{\Omega}(0) = -\tau \text{ and } \tilde{\Omega} = \tilde{\Omega}(0), \tag{15}$$

where (and hereafter) i is the imaginary unit, $\tilde{u} = u_x + iu_y$, $\tilde{\Omega} = \Omega_x + i\Omega_y$, $S = k_1 g \rho^{*'} / 4(\gamma + \kappa)$, $\tilde{\nabla} = \partial/\partial x + i\partial/\partial y$ and the prime denotes differentiation with respect to z .

(b) For $\tilde{\nabla} p = 0$ from Eq. 13 we have

$$\int_0^\infty \tilde{u} dz = \frac{i\tau}{\rho f}, \tag{16}$$

which coincides with the integral volume transport of the classical Ekman model.

3.3.2 Unstratified flow

Let us firstly consider the compliance of the flow situation described by Eqs. 13 and 14 for $S = 0$ with the Stokes drift effect [26,27]. For monochromatic surface waves with amplitude a , wavenumber k_w and wave phase speed c the Stokes drift effect results in a flow velocity determined by

$$\tilde{u} = U_S \exp\left(-\frac{z}{\ell_w}\right), \tag{17}$$

where $\ell_w = 1/2k_w$ and $U_S = c(ak_w)^2$. It is easy to make sure that Eq. 17 agrees with Eq. 14 for $\ell = (\vartheta J/4\kappa)^{1/2} = \ell_w$, and $\tilde{\Omega} \equiv \tilde{\omega} = 1/2i\tilde{u}'$. Based on this model outcome we shall adopt for the value of the depth scale ℓ in the open ocean the estimate $\ell = \ell_w = 5 \text{ m}$ [27].

Consider now the case with $\vartheta J = 0$, then from Eq. 14 we have

$$\tilde{\Omega} = \frac{i\gamma}{2(\gamma + \kappa)} \tilde{u}' \tag{18}$$

and Eq. 13 reduces to $\mu_{ef}\tilde{u}'' + i\rho f\tilde{u} = 0$, which coincides with the equation of the classical Ekman model with the shear viscosity replaced by $\mu_{ef} = \gamma\kappa/(\gamma + \kappa)$ and with the Ekman depth scale specified as $\ell_E = (2\mu_{ef}/\rho f)^{1/2}$. In the following we will make use of this result assigning ℓ_E the value of about 30 m typical for the Ekman depth scale at midlatitudes in the open ocean [34].

Assuming henceforth $\tilde{\nabla} p = 0$, if the stratification effects are neglected ($S = 0$), the solution of Eqs. 13 and 14 is

$$\tilde{u} = \tilde{C}_1 \exp(\lambda_1 z) + \tilde{C}_2 \exp(\lambda_2 z), \tag{19}$$

$$\tilde{\Omega} = \frac{i}{2} \left(1 - \frac{\mu_{ef}}{\gamma}\right) \left[\frac{\lambda_1}{1 - (\mu_{ef}/\gamma)\ell^2\lambda_1^2} \tilde{C}_1 \exp(\lambda_1 z) + \frac{\lambda_2}{1 - (\mu_{ef}/\gamma)\ell^2\lambda_2^2} \tilde{C}_2 \exp(\lambda_2 z) \right], \tag{20}$$

where λ_1 and λ_2 are the roots of the biquadratic equation

$$\lambda^4 - \left(\frac{1}{\ell^2} - 2i\frac{\mu_{ef}}{\gamma}\frac{1}{\ell_E^2}\right)\lambda^2 - 2i\frac{1}{\ell^2\ell_E^2} = 0 \tag{21}$$

with negative real parts, while \tilde{C}_1 and \tilde{C}_2 are complex integration constants. Using the equality

$$\left(1 - \frac{\mu_{ef}}{\gamma}\ell^2\lambda_2^2\right)\left(1 - \frac{\mu_{ef}}{\gamma}\ell^2\lambda_1^2\right) = 1 - \frac{\mu_{ef}}{\gamma},$$

which holds due to the properties of the solution of Eq. 21, Eq. 20 can be written also as

$$\tilde{\Omega} = \frac{i}{2} \left[\left(1 - \frac{\mu_{ef}}{\gamma}\ell^2\lambda_2^2\right)\lambda_1\tilde{C}_1 \exp(\lambda_1 z) + \left(1 - \frac{\mu_{ef}}{\gamma}\ell^2\lambda_1^2\right)\lambda_2\tilde{C}_2 \exp(\lambda_2 z) \right]. \tag{22}$$

In the following we assume that \tilde{C}_1 and \tilde{C}_2 in Eqs. 19 and 22 are determined for $\tilde{\Omega}$ collinear at $z = 0$ with the vorticity $\tilde{\omega} = 1/2i\tilde{u}'$. This assumption is formalized by $\tilde{\Omega}(0) = k_2\tilde{\omega}(0)$, where k_2 is a scalar coefficient quantifying the boundary condition for $\tilde{\Omega}$ at $z = 0$. The assumption results in

$$\tilde{u}'(0) = -\frac{1}{\gamma(1 - k_2)}\tau \quad \text{and} \quad \tilde{\Omega}(0) = -\frac{i}{2}\frac{k_2}{\gamma(1 - k_2)}\tau \tag{23}$$

determining \tilde{C}_1 and \tilde{C}_2 as

$$\tilde{C}_1 = \frac{\tau}{\lambda_1\mu_{ef}} \left[1 - \frac{1}{1 - k_2}\frac{\mu_{ef}}{\gamma}\ell^2\lambda_1^2 \right] \frac{1}{(\lambda_1^2 - \lambda_2^2)\ell^2} \tag{24}$$

and

$$\tilde{C}_2 = \frac{\tau}{\lambda_2\mu_{ef}} \left[-1 + \frac{1}{1 - k_2}\frac{\mu_{ef}}{\gamma}\ell^2\lambda_2^2 \right] \frac{1}{(\lambda_1^2 - \lambda_2^2)\ell^2}. \tag{25}$$

For the estimates for ℓ and ℓ_E adopted above (determining also μ_{ef}) the derived solution appears depending on two parameters—on k_2 (quantifying the boundary condition for $\tilde{\Omega}$) and on the coefficient of turbulence rotational viscosity γ (or μ_{ef}/γ).

In the following, a sequence of two approximations of the solution for the velocity in Eq. 19 are considered. The approximations correspond to the characteristic values of ℓ and ℓ_E adopted above.

The first approximation assumes that $(\ell/\ell_E)^4 \ll 1$. Under this assumption the terms of order $(\ell/\ell_E)^4$ are neglected. Hence, the Taylor series $\exp(i\alpha\ell^2/\ell_E^2) = \sum_{n=1}^{\infty} (i\alpha\ell^2/\ell_E^2)^n/n!$ becomes equal, in this approximation, to $1 + i\alpha\ell^2/\ell_E^2$ (α is an arbitrary real quantity of order 1). This approximation determines λ_1 and λ_2 :

$$\lambda_1^2 = \frac{1}{\ell^2} \exp\left(2i\left(1 - \frac{\mu_{ef}}{\gamma}\right) \frac{\ell^2}{\ell_E^2}\right), \quad \lambda_2^2 = -2i \frac{1}{\ell_E^2} \tag{26}$$

giving

$$\lambda_1 = -\frac{1}{\ell} \exp\left(i\left(1 - \frac{\mu_{ef}}{\gamma}\right) \frac{\ell^2}{\ell_E^2}\right), \quad \lambda_2 = \frac{i-1}{\ell_E} \tag{27}$$

Equation 27 specifies the first and the second terms in Eq. 19 as the Stokes and the Ekman velocity constituents, respectively,

$$\tilde{u}_S = \tilde{u}_S(0)\exp(\lambda_1 z), \tag{28}$$

$$\tilde{u}_E = \tilde{u}_E(0)\exp(\lambda_2 z), \tag{29}$$

where (and henceforth) \tilde{C}_1 and \tilde{C}_2 are denoted by $\tilde{u}_S(0)$ and $\tilde{u}_E(0)$. As applied to Eqs. 24 and 25 the approximation results in

$$\tilde{u}_S(0) = \frac{\tau\ell}{\mu_{ef}(1-k_2)} \left[k_2 - 1 + \frac{\mu_{ef}}{\gamma} \exp\left(2i\left(1 - \frac{\mu_{ef}}{\gamma}\right) \frac{\ell^2}{\ell_E^2}\right) \right] \exp\left(i\left(-5 + 3\frac{\mu_{ef}}{\gamma}\right) \frac{\ell^2}{\ell_E^2}\right) \tag{30}$$

and

$$\tilde{u}_E(0) = \frac{\tau\ell_E}{\sqrt{2}\mu_{ef}(1-k_2)} \left[-k_2 + \exp\left(2i\frac{\mu_{ef}}{\gamma} \frac{\ell^2}{\ell_E^2}\right) \right] \exp\left(i\left[\frac{\pi}{4} + \left(-4 + 2\frac{\mu_{ef}}{\gamma}\right) \frac{\ell^2}{\ell_E^2}\right]\right). \tag{31}$$

The second approximation assumes the ratio ℓ^2/ℓ_E^2 to be sufficiently small that $\exp(i\alpha\ell^2/\ell_E^2)$ may be approximated by 1. Under this assumption, the expression for λ_1 in Eq. 27 is replaced by $\lambda_1 = -1/\ell$ and Eqs. 30 and 31 would be replaced by

$$\tilde{u}_S(0) = \frac{\tau\ell}{\mu_{ef}(1-k_2)} \left[k_2 - 1 + \frac{\mu_{ef}}{\gamma} \right] \tag{32}$$

and

$$\tilde{u}_E(0) = -\frac{\tau}{\lambda_2\mu_{ef}} = \frac{\tau\ell_E}{\sqrt{2}\mu_{ef}} \exp(i\pi/4). \tag{33}$$

The derived solutions follow from Eqs. 13–15 set up for the Northern Hemisphere. These solutions hold also for the Southern Hemisphere if the y-axis is reversed to the opposite direction, forming a left-hand coordinate system (x, y, z).

We start the analysis of the derived solution from the second approximation. This approximation specifies k_2 as having the values from the interval $[1 - \mu_{ef}/\gamma, 1]$. For $k_2 = 1 - \mu_{ef}/\gamma$ we have $\tilde{u}_S = 0$ and $\tilde{u} = \tilde{u}_E$, i.e., the solution reduces to the classical Ekman solution, and for $k_2 = 1$ we have $\tilde{u}_E = 0$ (equivalent to neglecting the Coriolis term in Eq. 13) and $\tilde{u} = \tilde{u}_S$, corresponding to the Stokes drift situation. The latter case assumes $\tau = 0$ with the indeterminate ratio $\tau/(1 - k_2)$ equalized to $\tilde{u}'(0)$. The approximation agrees with the following

observed deviations from the solution of the classical Ekman model: that the veering of the surface drift velocity from the direction of the wind stress is less than $\pi/4$, the increase of the downwind velocity component and of the downwind velocity shear next to the surface as well as the non-collinearity of the stress and velocity shear in the Ekman layer (despite their assumed collinearity at the surface $z = 0$).

While in the second approximation the Ekman and Stokes velocity constituents are independent, within the first approximation these constituents appear interdependent. The interdependence shows in the dependence of $\tilde{u}_S(0)$ and $\tilde{u}_E(0)$ on both scale parameters, ℓ and ℓ_E . In particular, due to the interdependence of the Ekman and Stokes velocity constituents, the angle between the velocity constituent $\tilde{u}_E(0)$ and the wind direction differs from $\pi/4$ and the direction of the Stokes velocity constituent at $z = 0$ deviates from the wind direction. The latter deviation is accompanied by a small turn of the Stokes velocity constituent with depth in the direction opposite to the direction of rotation of the Ekman constituent reflected by the negative imaginary component of λ_1 .

Within both approximations the velocity rotational scale and its e -folding scale coincide below the “Stokes layer” leaving the description of the situations with different rotational and e -folding scales to the general solution not restricted by the smallness of ℓ in respect to ℓ_E . The latter situation may occur, for example, at high latitudes in the presence of relatively long surface waves.

Figure 2 compares the data from [24] (circles) measured in Drake Passage at depths from $z = 26$ m to $z = 90$ m in conditions of (presumably) negligible stratification with the Ekman constituent of the velocity calculated from Eq. 29 for $\text{Re } \tilde{u}_E - U$, where U is the estimated

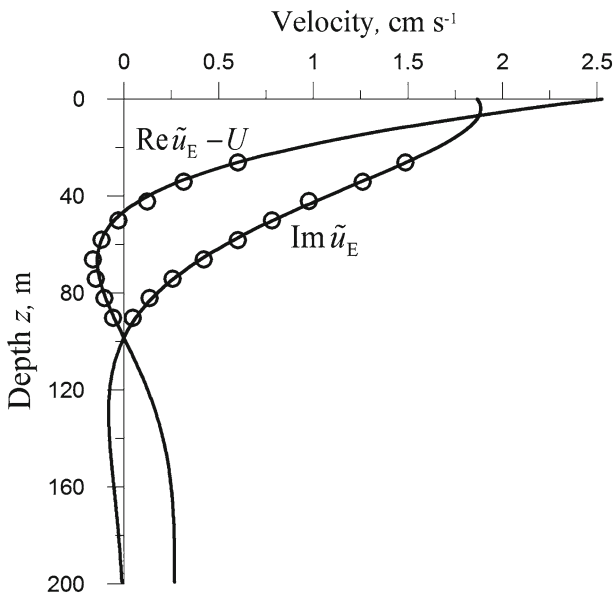


Fig. 2 The depth-dependence of the velocity components $\text{Re } \tilde{u}_E - U$, where $U = -0.25 \text{ cm s}^{-1}$ is the estimated reference velocity, and $\text{Im } \tilde{u}_E$ (solid curves), calculated from Eq. 29 for $\ell_E = 40 \text{ m}$, $\text{Re } \tilde{u}_E(0) = 2.276 \text{ cm s}^{-1}$ and $\text{Im } \tilde{u}_E(0) = 1.865 \text{ cm s}^{-1}$ compared with the respective velocity data (circles) adopted from [24]

velocity at an expected reference level (hereafter the reference velocity), and $\text{Im } \tilde{u}_E$ (curves). The calculations are performed for the e -folding scale of the Ekman layer estimated from the data and for $\tilde{u}_E(0)$ calculated by Eq. 29 from the velocity value observed at $z = 26.15$ m. The comparison confirms the applicability of the classical Ekman solution in the depth interval covered by the data in [24]. The only difference from the classical Ekman solution is the angle between the Ekman constituent of the flow velocity at $z = 0$ and the wind stress, since it is smaller than $\pi/4$. The smaller angle is explained within the model by the Stokes drift effect.

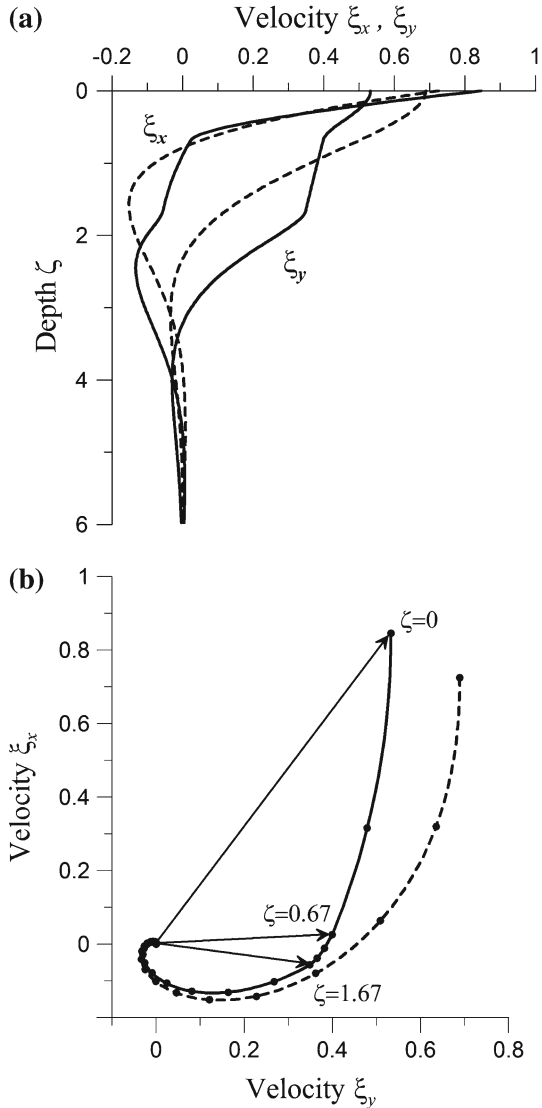
As much as the classical Ekman model matches the observed velocity distribution in Fig. 2, the velocity rotation and e -folding scales coincide and the turbulent stresses are collinear with the velocity shear in the data-covered depth interval. This implication evidently disagrees with the statements in [24] drawn from the same data set about the velocity rotation scale exceeding its e -folding scale by 2–3 times and about the non-collinearity of the velocity shear and turbulent stresses. Similar statements have been repeated also in several other papers cited in the Introduction. The disagreement follows from the misleading extension of the notion “ e -folding scale” in [24] to the data set from which the velocity at a presumable reference level is subtracted. Due to the subtraction, the resultant velocity vanishes at the reference level and the e -folding scale of velocity remains always smaller than the reference level depth. The non-collinearity, on the other hand, follows from ignoring the effect of non-zero velocity shear at the reference level if calculating turbulent stresses.

3.3.3 Stratified flow

The discussion in the previous subsection will now be complemented with the inclusion of the stratification effect ($S \neq 0$) presented by the term $4(\gamma + \kappa) S \tilde{\Omega}$ in Eq. 14. In Fig. 3 the vertical profiles of the velocity and the respective velocity spirals calculated from Eqs. 13–15 for $\nabla p = 0$, for the non-stratified ocean, $S \equiv 0$, (dashed curves) and for the stratified ocean, $S = 5$, in the depth interval $0.67 < \zeta = z/\ell_E < 1.67$ with $S = 0$ elsewhere, (solid curves) are compared. The calculations are performed for the characteristic thicknesses of the Stokes and the Ekman layers adopted above ($\ell = 5$ m, $\ell_E = 30$ m), for $\mu_{ef}/\gamma = 0.1$ and $k_2 = 0.9$. Let us draw attention to the following effects. Firstly, similar to the Stokes drift effect, the presence of a density jump layer (pycnocline) decreases the veering of the flow velocity vector at $z = 0$ from the direction of the wind stress. Secondly, in the pycnocline the decrease of the norm of the velocity vector as well as its rotation with depth is smaller than in the regions adjacent to the pycnocline, or, in other words, the pycnocline layer moves more like a slab, compared to the flow in adjacent depth intervals. The latter effects are reflected also in the velocity spiral (Fig. 3b), where the velocity vectors in the pycnocline at the depths $0.67 < \zeta < 1.67$ prove closer to each other than the vectors from the immediate neighbouring depths.

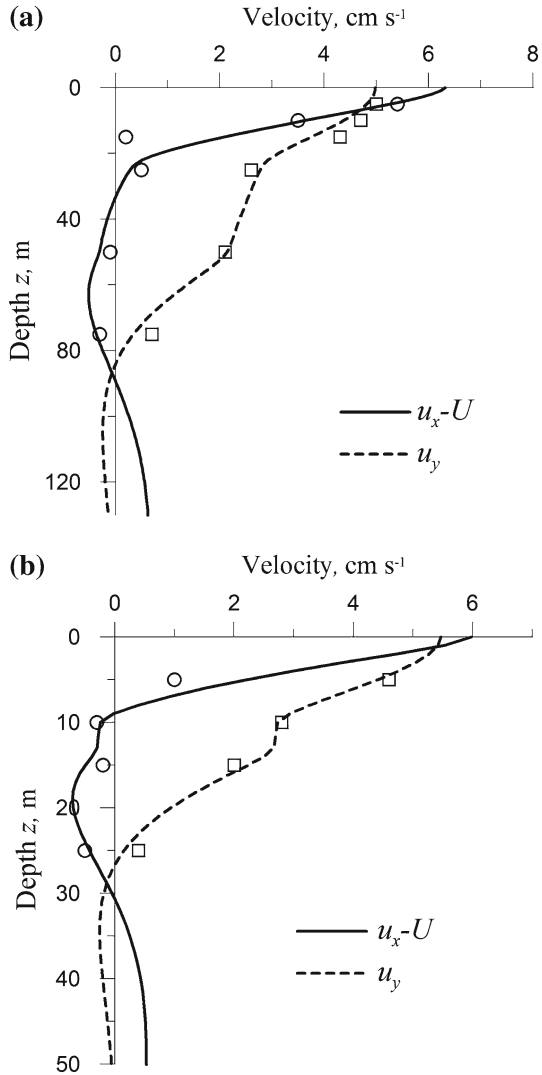
The calculated vertical profiles of $u_x - U$ (solid curves), where U is the reference velocity, and of u_y (dashed curves) calculated from Eqs. 13–15 are compared in Fig. 4 with the data from [33] collected in summer and winter conditions. The comparison confirms the effects outlined above of stratification of the velocity profiles. The reference velocities U , the ocean stratification conditions (specified within the model by S) and the boundary conditions at $z = 0$ are not reported in [33], therefore the comparison just shows the applicability of the model situation shown in Fig. 3a to the actual observed velocity profiles different in summer and winter. In Fig. 4a (winter) $U = 0.48 \text{ cm s}^{-1}$ and $S = 1$ in the depth interval

Fig. 3 (a) Vertical profiles of velocity $\xi_x = u_x/|\bar{u}(0)|$, $\xi_y = u_y/|\bar{u}(0)|$ with stratification (solid curves) and with no stratification (dashed curves) dependent on the depth $\zeta = z/\ell_E$ and (b) velocity spiral (curve with dots over every interval of 0.333 of the depth ζ) corresponding to the velocity profile in stratified medium in the panel (a) with arrows highlighting velocities at three indicated depths. All calculations are performed for Ω and ω aligned at $z = 0$, for $\mu_{ef}/\gamma = 0.1$, $\ell_E = 30$ m, $\ell = 5$ m, $k_2 = 0.9$, $S = 0$ for the non-stratified medium and $S = 5$ in the depth interval $0.67 < \zeta < 1.67$ for the stratified medium



23 m < z < 50 m with $S \ll 1$ elsewhere; in Fig. 4b (summer) $U = 0.6 \text{ cm s}^{-1}$ and $S = 1$ in the depth interval 10 m < z < 13 m with $S \ll 1$ elsewhere. The values of S applied in the calculation reflect the typical stratification conditions in the region in the summer and winter situations. In all calculations the ratio τ/μ_{ef} was kept equal to 0.05 s^{-1} entailing the proportionality of μ_{ef} as well as of the squared Ekman length scale ℓ_E^2 to the wind stress τ . The rest of the “model parameters” are specified as follows: in Fig. 4a $\mu_{ef}/\gamma = 0.09$, $\ell_E = 27$ m, $\ell = 5$ m and $k_2 = 0.1$; in Fig. 4b $\mu_{ef}/\gamma = 0.024$, $\ell_E = 10$ m, $\ell = 1$ m and $k_2 = 0.4$. The values of μ_{ef}/γ , ℓ_E and ℓ in winter are larger and k_2 is smaller than their values in summer indicating that τ is larger and the ocean surface is rougher in winter conditions.

Fig. 4 Calculated vertical profiles of $u_x - U$ and u_y for stratified ocean (curves), together with the data adopted from [33] on downwind (circles) and crosswind (squares) velocity components in winter (a) and summer (b) situations. Calculations are performed for $\tau/\mu_{ef} = 0.05 \text{ s}^{-1}$ and in (a) for $U = 0.6 \text{ cm s}^{-1}$, $\mu_{ef}/\gamma = 0.09$, $\ell_E = 10 \text{ m}$, $\ell = 1 \text{ m}$, $k_2 = 0.1$, $S = 1$ in the interval $23 \text{ m} < z < 50 \text{ m}$ and $S \ll 1$ elsewhere; in (b) $U = 0.48 \text{ cm s}^{-1}$, $\mu_{ef}/\gamma = 0.024$, $\ell_E = 10 \text{ m}$, $\ell = 1 \text{ m}$, $k_2 = 0.4$, $S = 1$ in the interval $10 \text{ m} < z < 13 \text{ m}$ and $S \ll 1$ elsewhere



4 Conclusion

The suggested model is set up to complement the classical Ekman layer model by including the Stokes drift and stratification effects. The model proceeds from the theory of Rotationally Anisotropic Turbulence (RAT) enhancing the methods of turbulence mechanics by accounting for the effects of the prevailing orientation of large-scale turbulent eddy rotation receiving its energy immediately from the average flow. The model explains the flow situation depending (in addition to the boundary and stratification conditions) on the characteristic depth of the Stokes drift layer, on the Ekman depth scale (which can be estimated as equal to the velocity rotation scale determined from the velocity data below the “Stokes layer”) and on one physical coefficient specified as the coefficient of turbulence rotational viscosity. According to the suggested model the additional effects incorporated in the model are: (a)

an increase in the downwind component of the velocity shear at the surface, (b) a decrease in the angle between the surface wind stress and the surface drift velocity, (c) that the velocity shear and stresses in the “Stokes layer” are non-collinear with the wind stress. The suggested model includes also the case where the velocity rotational depth scale exceeds its e -folding depth scale, however it disagrees with the reasoning and the extent of the difference of the scales declared in [24].

References

1. Ariman T, Turk MA, Silvester DO (1973) Microcontinuum fluid mechanics—review. *Int J Eng Sci* 11:905–930
2. Chereskin TK (1995) Direct evidence for an Ekman balance in the California Current. *J Geophys Res* 100:18261–18269
3. Chereskin TK, Price JF (2001) Ekman transport and pumping. In: Steele J, Thorpe S, Turekian K (eds) *Encyclopedia of ocean sciences*. Academic Press, San Diego pp 809–815
4. Coleman GN, Ferziger JH, Spalart PR (1990) A numerical study of the turbulent Ekman layer. *J Fluid Mech* 213:313–348
5. Cushman-Roisin B (1994) *Introduction to geophysical fluid dynamics*. Prentice Hall, Englewood Cliffs
6. Dahler JS, Scriven LF (1961) Angular momentum of continua. *Nature* 192:36–37
7. Ekman VW (1905) On the influence of the Earth’s rotation on ocean currents. *Ark Mat Astr Fys* 2: 1–53
8. Eringen AC (1966) Theory of micropolar fluids. *J Math Mech* 16:1–18
9. Eringen AC (1968) Mechanics of micromorphic continua. In: Kröner E (ed) *Mechanics of generalized continua*. Springer, Berlin pp 18–33
10. Heinloo J (1985) Phenomenological mechanics of turbulent flows. Valgus, Tallinn (in Russian)
11. Heinloo J (1999) Mechanics of turbulence. Estonian Academy of Sciences, Tallinn (in Russian)
12. Heinloo J (2004) The formulation of turbulence mechanics. *Phys Rev E* 69. doi:[10.1103/PhysRevE.69.056317](https://doi.org/10.1103/PhysRevE.69.056317)
13. Heinloo J (2006) Eddy-driven flows over varying bottom topography in natural water bodies. *Proc Estonian Acad Sci Phys Math* 55:235–245
14. Heinloo J (2008) The description of externally influenced turbulence accounting for a preferred orientation of eddy rotation. *Eur Phys J B* 62:471–476
15. Heinloo J, Toompuu A (2004) Antarctic Circumpolar Current as a density-driven flow. *Proc Estonian Acad Sci Phys Math* 53:235–265
16. Heinloo J, Toompuu A (2006) Modeling a turbulence effect in formation of the Antarctic Circumpolar Current. *Ann Geophys* 24:3191–3196
17. Heinloo J, Toompuu A (2007) Eddy-to-mean energy transfer in geophysical turbulent jet flows. *Proc Estonian Acad Sci Phys Math* 56:283–294
18. Heinloo J, Toompuu A (2008) Modeling turbulence effect in formation of zonal winds. *Open Atmos Sci J* 2:249–255
19. Heinloo J, Toompuu A (2009) A model of average velocity in oscillating turbulent boundary layers. *J Hydraul Res* 47:676–680
20. Heinloo J, Toompuu A (2010) A model of vertical distribution of suspended matter in an open channel flow. *Environ Fluid Mech* (online first). doi:[10.1007/s10652-010-9180-1](https://doi.org/10.1007/s10652-010-9180-1)
21. Heinloo J, Toompuu A (2010) A model of vertical distribution of suspended sediment in the bottom layer of a natural water body. *Estonian J Earth Sci* 59:238–245
22. Heinloo J, Võsumaa Ü (1992) Rotationally anisotropic turbulence in the sea. *Ann Geophys* 10:708–715
23. Huang NE (1979) On surface drift currents in the ocean. *J Fluid Mech* 91:191–208
24. Lenn Y-D, Chereskin TK (2009) Observations of Ekman currents in the Southern Ocean. *J Phys Oceanogr* 39:768–779
25. Madsen OS (1977) A realistic model of the wind-induced Ekman boundary layer. *J Phys Oceanogr* 7: 248–255
26. Phillips OM (1977) *Dynamics of the upper ocean*. Cambridge University Press, Cambridge
27. Polton JA, Lewis DM, Belcher SE (2005) The role of wave-induced Coriolis–Stokes forcing on the wind-driven mixed layer. *J Phys Oceanogr* 35:444–457
28. Price JF, Sundermeyer MA (1999) Stratified Ekman layers. *J Geophys Res* 104(C9):20467–20494
29. Price JF, Weller RA, Pinkel R (1986) Diurnal cycling: observations and models of the upper ocean response to diurnal heating, cooling, and wind mixing. *J Geophys Res* 91:8411–8427

30. Price JF, Weller RA, Schudlich RR (1987) Wind-driven ocean currents and Ekman transport. *Science* 238:1534–1538
31. Richman JG, deSzoeke RA, Davis RE (1987) Measurements of near-surface shear in the ocean. *J Geophys Res* 92:2851–2858
32. Sedov LI (1971) *A course in continuum mechanics*. Wolters-Noordhoff, Groningen
33. Schudlich RR, Price JF (1998) Observations of seasonal variation in the Ekman layer. *J Phys Oceanogr* 28:1187–1204
34. Stewart RH (2005) *Introduction to physical oceanography*. Texas A&M University, Texas. http://oceanworld.tamu.edu/resources/ocng_textbook/contents.html. Accessed 15 Dec 2010
35. Toompuu A, Heinloo J, Soomere T (1989) Modeling the Gibraltar salinity anomaly. *Okeanologiya* 29:939–945
36. Võsumaa Ü, Heinloo J (1996) Evolution model of the vertical structure of the active layer of the sea. *J Geophys Res* 101:25635–25646
37. Weller RA (1981) Observations of the velocity response to wind forcing in the upper ocean. *J Geophys Res* 86:1969–1977
38. Wijffels S, Firing E, Bryden HL (1994) Direct observations of the Ekman balance at 10° in the Pacific. *J Phys Oceanogr* 24:1666–1679
39. Zikanov O, Slinn DN, Dhanak MR (2003) Large-eddy simulations of the wind-induced turbulent Ekman layer. *J Fluid Mech* 495:343–368